






Article

Combining Proximal and Remote Sensors in Spatial Prediction of Five Micronutrients and Soil Texture in a Case Study at Farmland Scale in Southeastern Brazil

Luiza Maria Pereira Pierangeli ¹ , Sérgio Henrique Godinho Silva ¹, Anita Fernanda dos Santos Teixeira ¹ , Marcelo Mancini ¹ , Renata Andrade ¹, Michele Duarte de Menezes ¹, João José Marques ¹, David C. Weindorf ^{2,*}  and Nilton Curi ¹ 

¹ Department of Soil Science, Federal University of Lavras, Lavras 37200-900, Minas Gerais, Brazil

² Department of Earth and Atmospheric Sciences, Central Michigan University, Mount Pleasant, MI 48859, USA

* Correspondence: weind1dc@cmich.edu; Tel.: +1-989-774-6467

Abstract: Despite the increasing adoption of proximal sensors worldwide, rare works have coupled proximal with remotely sensed data to spatially predict soil properties. This study evaluated the contribution of proximal and remotely sensed data to predict soil texture and available contents of micronutrients using portable X-ray fluorescence (pXRF) spectrometry, magnetic susceptibility (MS), and terrain attributes (TA) via random forest algorithm. Samples were collected in Brazil from soils with high, moderate, and low weathering degrees (Oxisols, Ultisols, Inceptisols, respectively), and analyzed by pXRF and MS and for texture and available micronutrients. Seventeen TA were generated from a digital elevation model of 12.5 m spatial resolution. Predictions were made via: (i) TA; (ii) TA + pXRF; (iii) TA + MS; (iv) TA + MS + pXRF; (v) MS + pXRF; and (vi) pXRF; and validated via root mean square error (RMSE) and coefficient of determination (R^2). The best predictions were achieved by: pXRF dataset alone for available Cu ($R^2 = 0.80$) and clay ($R^2 = 0.67$) content; MS + pXRF dataset for available Fe ($R^2 = 0.68$) and sand ($R^2 = 0.69$) content; TA + pXRF + MS dataset for available Mn ($R^2 = 0.87$) content. pXRF data were key to the best predictions. Soil property maps created from these predictions supported the adoption of sustainable soil management practices.

Keywords: digital soil mapping; pXRF; terrain attributes; tropical soils; Oxisols; Ultisols; Inceptisols; random forest



Citation: Pierangeli, L.M.P.; Silva, S.H.G.; Teixeira, A.F.d.S.; Mancini, M.; Andrade, R.; de Menezes, M.D.; Marques, J.J.; Weindorf, D.C.; Curi, N. Combining Proximal and Remote Sensors in Spatial Prediction of Five Micronutrients and Soil Texture in a Case Study at Farmland Scale in Southeastern Brazil. *Agronomy* **2022**, *12*, 2699. <https://doi.org/10.3390/agronomy12112699>

Academic Editor:
Pablo Martín-Ramos

Received: 21 September 2022

Accepted: 26 October 2022

Published: 31 October 2022

Publisher's Note: MDPI stays neutral with regard to jurisdictional claims in published maps and institutional affiliations.



Copyright: © 2022 by the authors. Licensee MDPI, Basel, Switzerland. This article is an open access article distributed under the terms and conditions of the Creative Commons Attribution (CC BY) license (<https://creativecommons.org/licenses/by/4.0/>).

1. Introduction

Detailed and accurate information on micronutrient availability plays an important role in crop production since deficiency or toxicity thresholds are much more limited than for macronutrients. Micronutrient deficiencies are an emerging limiting factor commonly reported in croplands of Brazil [1,2]. This issue is also influenced by lime application for soil pH adjustment, a common and indispensable practice in many tropical region soils, which can decrease the availability of plant micronutrients. In tropical regions, there is a scarcity of massive data acquisition, detailed modeling, and spatial prediction of micronutrients.

Soil texture is a major factor affecting micronutrient availability to plants, especially under tropical conditions [3]. Moreover, soil texture is also an important driver of soil fertility and water dynamics [4]. In South American countries, soil testing is more commonly used to identify micronutrient disorders in crops [1]. Thus, assessing and mapping the current micronutrient status, as well as any other soil attributes affecting their availability can be a valuable source of information for better soil fertility management.

A map showing soil attribute variability is one of the most important data layers for precision farming [5] as spatial prediction is a key point for site-specific nutrient management [6,7]. However, when compared with traditional management, precision farming requires high sampling density to properly assist in site-specific management [5], which

is frequently constrained by the costs of traditional laboratory-based soil physicochemical analyses. Such analyses are also time-consuming, laborious, and non-environmentally friendly, as they utilize chemical reagents and generate chemical wastes requiring proper disposal. Thus, using alternative methods that enable the characterization of soil samples quickly, economically, and without the generation of chemical effluents is preferable. This desirable combination can be obtained via remote and, in the last 20 years, proximal sensing analyses [8].

Recently, proximal sensors such as portable X-ray fluorescence (pXRF) spectrometry and magnetic susceptibility (MS), as well as digital elevation models (DEMs) obtained from satellite data and their products (remote sensing data) have become promising alternatives for soil characterization [9,10]. In seconds, pXRF can identify and quantify total elemental contents in the soil, as each element produces element-specific fluorescent energy allowing for elemental identification; the intensity of said energy provides elemental quantification [11,12]. Recently, tremendous advances in pXRF application in tropical soils have been reported for the characterization and prediction of their attributes [13–18].

By comparison, MS is an important soil attribute related to the concentration of magnetic iron oxides, reflecting different iron oxide mineral forms and dynamics [19]. In tropical regions, MS affords solid capabilities in assessing soil parent material [20,21] which influences soil physicochemical attributes [22]. Both MS and pXRF methods are non-invasive, non-destructive, and can be used under field or laboratory conditions. Although most soil studies have been conducted using pXRF and MS data separately, their combination for soil attribute prediction justifies further investigation, especially across highly heterogeneous areas [23].

From the soil attributes spatial prediction perspective, most studies have applied a digital soil mapping framework, supported by soil = $f(\text{SCORPAN} + \epsilon)$ predictive model (S—inherent soil, C—climate, O—organisms, R—relief, P—parent material, A—age, N—geographical location of the area or point of interest along with ϵ —error component assessment) based upon Jenny [24] and expanded later by McBratney et al. [25]. Thus, soil–environment relationships can be established via quantitative models (e.g., machine learning techniques), using digital proxies of soil-forming factors as environmental predictor covariates.

PXRF and MS (proxies of S and P) have been used together with other variables for soil attribute spatial prediction [9,15]. Relief information can be accessed easily via DEM and DEM-derived topographic features, the so-called terrain attributes such as slope, topographic wetness index, etc. [15]. These variables are most commonly applied in spatial predictive models for digital soil mapping since they drive water and nutrients dynamics, soil erosion, and pedogenesis [25–29]. Data fusion can aid in obtaining information on soil attributes across the landscape [30] and improve the precision of site-specific management [31]. Machine learning algorithms capable of depicting relations between predictors and the target variable enhance this procedure [32–35].

The potential application of this approach based on the fusion of proximal and remotely sensed data to enhance soil attribute characterization both locally and spatially as well as the lack of studies evaluating the combination of such sensor data motivated this study. As such, the objectives of this study were to: (1) characterize soils in a highly heterogeneous research farm in Brazil with diverse land uses via pXRF, MS, and terrain attributes; (2) predict soil available B, Cu, Fe, Mn, and Zn, and clay, silt, and sand contents via pXRF, MS, and TA data separately and combined; and (3) produce spatial predictions of available micronutrient content and texture for the soils of the study area. B, Cu, Fe, Mn, and Zn were investigated herein since most micronutrient deficiencies in Brazilian crops are related to these five elements. The other micronutrients (Cl, Mo, and Ni) are either applied as fertilizers commonly used in Brazil (e.g., KCl), become more available with liming (common management practice in Brazil) or the natural contents in Brazilian soils are adequate for most crops in addition to the very small amount required by plants [2,4]. We hypothesize that robust and accurate prediction models and maps will be delivered

for soil micronutrient availability and soil texture by at least one of the aforementioned approaches, despite diverse soil classes and several land uses across the study area.

2. Materials and Methods

2.1. Study Area

The study was conducted at the Palmital Research farm (Figure 1), Federal University of Lavras, located in the municipality of Ijaci, Minas Gerais, Brazil, between UTM longitudes 506,793 and 508,882 mE and latitudes 7,659,470 and 7,660,685 mN, zone 23 K, datum SIRGAS 2000. The main soil classes are Oxisols, Ultisols, and Inceptisols, representing the major Brazilian soils and a classical decreasing sequence of pedogenetic development. The land uses include native vegetation (Subperennial tropical forest) and different types of field experiments and crops: eucalyptus, mahogany, slash pine, soybean, maize, common bean, and forage grass (*Eucalyptus* sp., *Swietenia macrophylla*, *Pinus* sp., *Glycine max*, *Zea mays*, *Phaseolus vulgaris*, and *Brachiaria decumbens*, respectively), under diverse management systems. This area covers 117 ha at an altitude of 814 to 866 m amsl. Lithology includes Precambrian gneiss, limestone, phyllite, and alluvial sediments from the Quaternary period [36]. The climate is humid semitropical featuring dry winters and rainy summers (Köppen classification: Cwa) with a mean annual temperature of 21 °C and mean annual precipitation of 1500 mm [37].

2.2. Soil Sampling and Laboratory Analyses

Samples from the A and B soil horizons were collected at 39 sites following a regular-grid design with 173 m of distance between them, totaling 78 samples (Figure 1), making up a density of one sample/3 ha (detailed mapping). Samples from A and B horizons were collected from 0–20 cm and 40–60 cm of depth, respectively. As coarse material, grain size, and moisture can influence analyses, soil samples were air-dried, ground (milled to break small aggregates), and passed through a 2 mm sieve to remove particles bigger than sand size (2 mm), which is a common procedure for soil analyses [38–40]. Samples that underwent this procedure are usually referred to as air-dried fine earth (ADFE). Next, ADFE samples were subjected to laboratory analyses for the determination of available B, Cu, Fe, Mn, Zn, and clay, silt, and sand contents.

Available Cu, Fe, Mn, and Zn were extracted with Mehlich-1 solution [38] and their quantification was performed via atomic absorption spectrophotometry using an AA 800 (Perkin Elmer, Waltham, MA, USA) [39]. Available B was extracted by the hot water method [40] and determined by the Azomethine H colorimetric method [41]. Clay, silt, and sand contents were determined via pipette method [42].

A Bartington MS2B (Bartington Instruments Limited, Witney, England) susceptibilimeter was used for MS determination [43]. Measurements were performed at low frequency (0.47 kHz) in triplicate.

Total elemental analysis was performed using a Vanta series pXRF (Olympus, Waltham, MA, USA) spectrometer. The instrument scans samples via two beams in sequence. One whole scan was completed in 60 s utilizing Geochem mode [44]. The equipment features an Rh X-ray tube operating at 8–50 kV as the excitation source. Before scanning, the equipment was calibrated with a stainless steel factory calibration alloy coin.

From all elements detected by pXRF, 19 were selected to build models in this study. They were: Al, As, Ca, Cr, Cu, Fe, K, Mn, Ni, P, Pb, Rb, S, Si, Sr, Ti, V, Y, and Zn. The accuracy of the equipment was evaluated via scanning of standard reference materials 2710a and 2711a certified by the National Institute of Standards and Technology (NIST). The performed accuracy assessment consisted in comparing pXRF-provided contents with standard contents in certified samples. The calculated ratio between pXRF-provided contents and standard contents was called recovery values. The recovery values obtained by the equipment per element were calculated as follows: recovery value = elemental content determined by pXRF/certified elemental content of the reference material. Calculated recovery values of elements used in the modeling process were listed below to highlight

the accuracy of the equipment (2710a/2711a): Al (0.61/0.61), As (1.06/1.43), Ca (0.65/0.88), Cr (-/1.19), Cu (1.02/1.01), Fe (0.92/0.96), K (0.83/0.85), Mn (0.93/0.96), Ni (-/1.15), P (0.63/0.52), Pb (1.02/1.08), Rb (-/-), S (-/-), Si (0.57/0.61), Sr (0.96/0.96), Ti (0.90/0.94), V (-/0.93), Y (-/-), and Zn (1.00/1.06). Dashes (-) indicates that the element either has no certified content in the reference material or was not detected by pXRF.

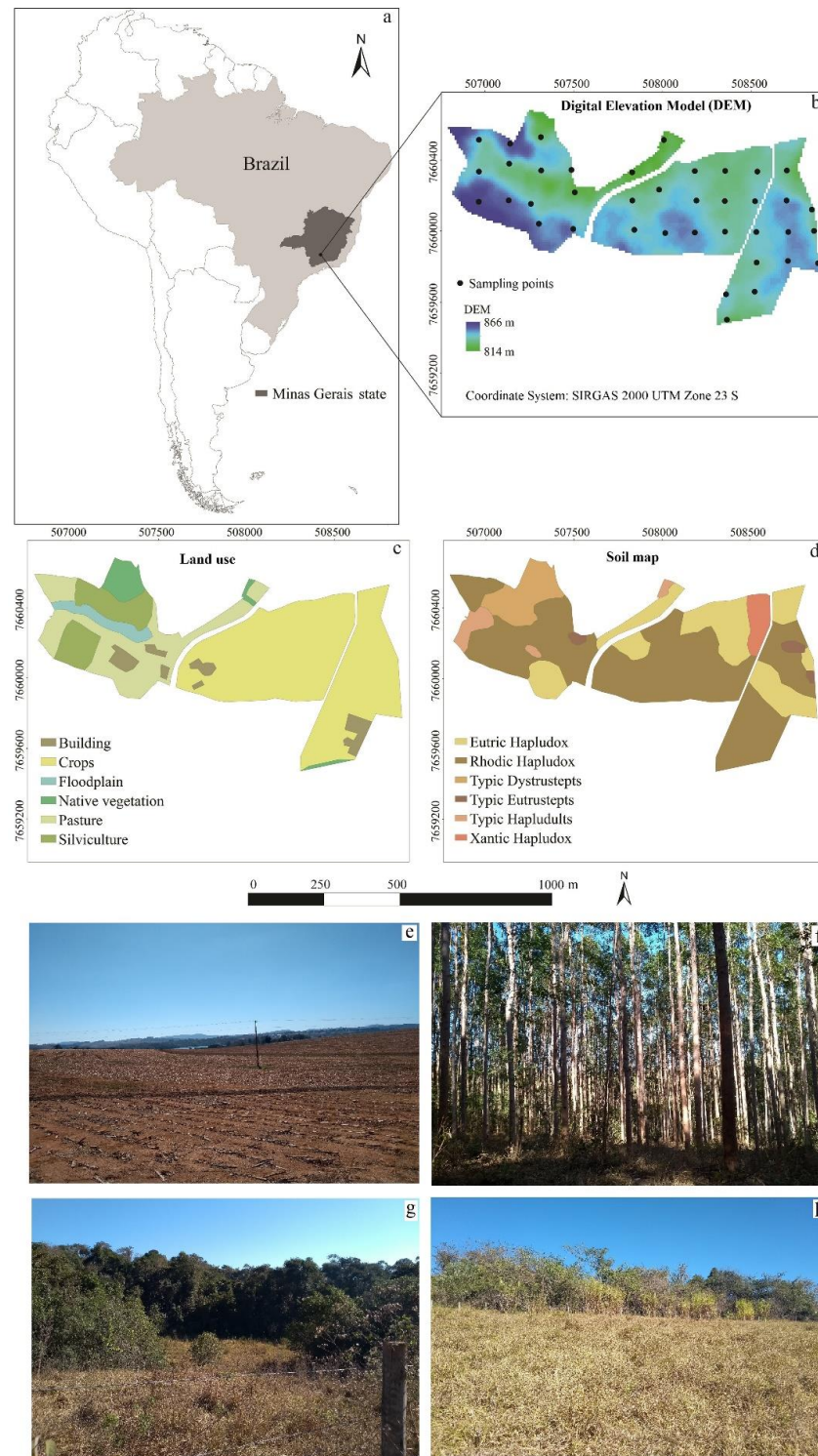


Figure 1. Location in Brazil (a), maps of sampling sites and elevation (b), land uses (c) and soil classes (d), and pictures of areas of crops (e), eucalyptus plantation (f), native vegetation (g), and pasture (h) in the study area at a farmland scale in Brazil.

2.3. Terrain Attributes

A DEM with 12.5 m resolution was obtained from ALOS PALSAR Global Radar Imagery (<https://search.asf.alaska.edu/#/> (accessed on 17 July 2021)). The TA derived from the DEM were calculated via SAGA GIS software (6.4.0) [45] and were selected based on several works that used TA for soil attribute prediction (please see [26,46–50] for more details on these TA), as follows: aspect (asp), catchment area (CA), catchment slope (CS), channel network base level (CNBL), closed depression (CD), convergence index (CI), cross-sectional curvature (CSC), flow accumulation (Flow), longitudinal curvature (LC), LS factor (lsf), modified catchment area (MCA), relative slope position (RSP), SAGA wetness index (SWI), slope (slp), topographic wetness index (TWI), valley depth (VD), and vertical distance to channel network (VDCN). Table 1 shows the variation of the terrain attributes selected for this study.

2.4. Modeling and Validation of the Predictions

A correspondence worksheet containing information on contents of soil micronutrients, soil texture, soil horizon, land use, pXRF, MS, and TA data for each sample was created to generate the full dataset. Land use may affect the contents of micronutrients in soil, e.g., by the addition of amendments and fertilizers in planted crops. Accordingly, land use was used as an explanatory variable to train all models due to its possible effect on the prediction of soil properties [51]. The “land use” variable includes all land use categories shown in Figure 1. Additionally, the “soil horizon” variable (indicating the horizon of each sample) was added to the datasets as a predictor variable for models created using samples from both A and B horizons for predictions, as previous studies pointed out that models per soil horizon provide different prediction accuracy [13,23]. The TA data were extracted from each sampling place by overlaying data with the sampling positions using a geographic information system (GIS).

Next, for the modeling process, all soil samples (78) were randomly separated into modeling and validation datasets, consisting of 70% (55 samples) and 30% (23 samples) of the total data, respectively, using cross-validation method imbedded in the caret package [52]. In addition, samples were subdivided and modeled into two ways: (i) specific models for A and B horizons separately, with number of samples = 39 for each (training = 27 samples, validation = 12 samples); and (ii) general model, including all 78 samples (the models’ so-called A + B horizons), with number of samples = 78, i.e., 55 and 23 samples for training and validation, respectively.

In order to adjust the models for predictions and to evaluate the importance of the predictors for the models, the pXRF, MS, and TA data were divided into six datasets considering predictor variables for soil micronutrients and texture prediction: (i) TA; (ii) TA + pXRF; (iii) TA + MS; (iv) TA + pXRF + MS; (v) MS + pXRF; and (vi) pXRF. So, 144 models were created and validated (6 predictor datasets × 3 horizon datasets × 8 target variables).

Random forest (RF) algorithm [33] was used to create the prediction models in R software (v.3.6.1) [52], using the caret package [53]. The following parameters were adopted based on the suggestions of Liaw and Wiener [54]: number of trees of the model (ntrees) = 1000, number of variables in each node (nodesize) = 5, and number of variables used in each tree (mtry) = 3. Moreover, the importance of each variable for model performance was calculated. This was completed by removing each variable from models and measuring the increase in prediction errors without each variable. The rationale behind this method is that a higher increase in mean square error (%IncMSE) occurs when an important predictor variable is removed from the model, since the removal of that variable caused more errors in the predictions. Thus, the greater the error increase (%IncMSE) by removing a variable from the model, the more important that variable is for the model. This is a powerful and significant measurement of the relative importance of each independent variable [54], promoting important data insights by ranking the order of importance of predictor variables.

Table 1. Descriptive statistics of terrain attributes at a farmland scale in Brazil.

Parameter	asp	CA	CD	CI	CNBL	CS	CSC	Flow	LC	lsf	MCA	RSP	slp	SWI	TWI	VD	VDCN
Min ^a	5.7×10^{-2}	144.0	0.0	−43.3	809.8	0.0	-7.9×10^{-3}	144.0	1×10^{-4}	0.0	282.5	2.2×10^{-3}	0.0	2.8	4.3	4×10^{-2}	0.1
Max ^b	6.3	3729.4	2.0	14.8	835.5	0.2	3.5×10^{-3}	12,665.6	5×10^{-3}	3.7	6982.1	1.0	25.3	7.7	11.8	34.5	35.3
Mean	3.3	788.7	0.5	−1.1	820.8	0.1	6×10^{-5}	1686.3	6×10^{-5}	1.3	1446.8	0.6	11.3	4.2	6.8	11.3	16.5
SD ^c	2.2	811.6	0.6	8.4	7.3	0.1	2×10^{-3}	2595.8	2×10^{-3}	1.0	1499.3	0.3	6.5	0.8	1.9	8.5	8.7
CV ^d	67.4	102.9	128.8	−773.1	0.9	49.2	−3290.9	153.9	3628.2	75.1	103.6	47.8	58.0	20.0	28.2	74.9	52.7

^a Minimum, ^b maximum, ^c standard deviation, ^d coefficient of variation. asp—aspect, CA—catchment area, CD—closed depression, CI—convergence index, CNBL—channel network base level, CS—catchment slope, CSC—cross-sectional curvature, Flow—flow accumulation, LC—longitudinal curvature, lsf—LS factor, MCA—modified catchment area, RSP—relative slope position, slp—slope, SWI—SAGA wetness index, TWI—topographic wetness index, VD—valley depth, VDCN—vertical distance to channel network.

The performance of each model was assessed via calculation of the coefficient of determination (R^2) and root mean square error (RMSE) between observed and predicted results of available micronutrients and sand, silt, and clay fraction contents. The greater the R^2 and the lower the RMSE values, the better the performance of the model.

The best prediction models for available B, Cu, Fe, Mn, Zn, and clay, silt, and sand fraction contents were used for spatial prediction throughout the study area. Since pXRF and MS data are point-based information (39 sampled locations), the multilevel B-splines interpolation method was applied [55] to make these variables continuously represented across the area. For this process, the data were imported into SAGA GIS, and the function “Multilevel B-splines” was applied. The values of the spatialized data were processed and extracted as a table containing their latitude/longitude information using ArcMap (10.1). Values of the predictor variables for the entire farm area were applied to the RF model created in R Studio (version 2022.07.01), generating the spatial prediction of the target soil attributes across the study area. Figure 2 presents a flowchart summarizing all the steps of this study.

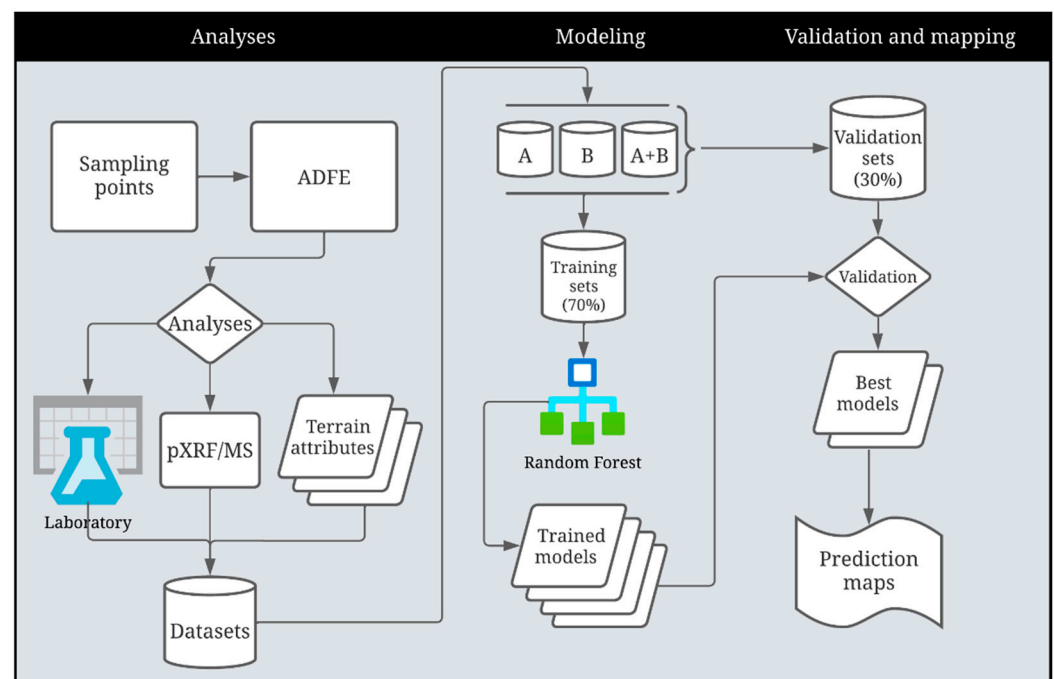


Figure 2. Flowchart illustrating the methods followed in this study, from laboratory and sensor analyses to modeling and digital soil mapping of micronutrients and soil texture at farmland scale in Brazil. ADFE—air-dried fine earth.

3. Results and Discussion

3.1. Characterization of Soil Attributes

For better visualization of the diversity of soils on the farm, soil samples were plotted within the soil textural triangle (Figure 3). Moreover, descriptive statistics of the soil attributes evaluated are shown in Table 2. Most samples presented a clayey texture. The mean clay, silt, and sand fraction contents (%) were 48, 18, and 34, respectively (Table 2). Clay fraction contents ranged from 27 to 74%, silt ranged from 1 to 36%, while sand ranged from 9 to 55%. Silt content was much lower than clay and sand contents, as expected because it is the most unstable fraction in most tropical soils [4]. Silva et al. [56] analyzed 1565 soil samples collected across Brazil and found a wide range of soil textures, especially represented by low contents of silt and greater contents of either clay or sand fractions, similarly to the results of this study. The coefficient of variation (CV) for particle size fractions was $\geq 20\%$ in most cases (especially the silt fraction), as expected due to the large

variation of soil classes and parent materials [57–59]. The large clay percentage in the soils is mostly related to low quartz content in the parent materials [60] and high degree of soil weathering.

The descriptive statistics of the micronutrient contents show high variability justified by the different soil classes, parent materials, and land uses (Table 2). Considering the range of micronutrient contents and their classes of agronomical interpretation in terms of availability for crops (from very low to very high contents), the contents of available B and Fe are mostly classified as low and very high, respectively [62]. Available Cu, Mn, and Zn contents varied from very low to high, reflecting the low natural fertility of soils under native vegetation on one side and soils that received ameliorant applications on another side (Figure 1c). The latter situation is also responsible for the greatest mean micronutrient contents in the A horizon for available B, Cu, and Zn. Other studies evaluating cultivated soils produced similar results [63–65]. Greater contents of available Fe and Mn may be related to the position of the soils in the landscape, as lowland areas tend to accumulate water, causing reduction and destabilization of Fe and Mn oxide minerals and, hence, an increase in available Fe and Mn in these areas [10].

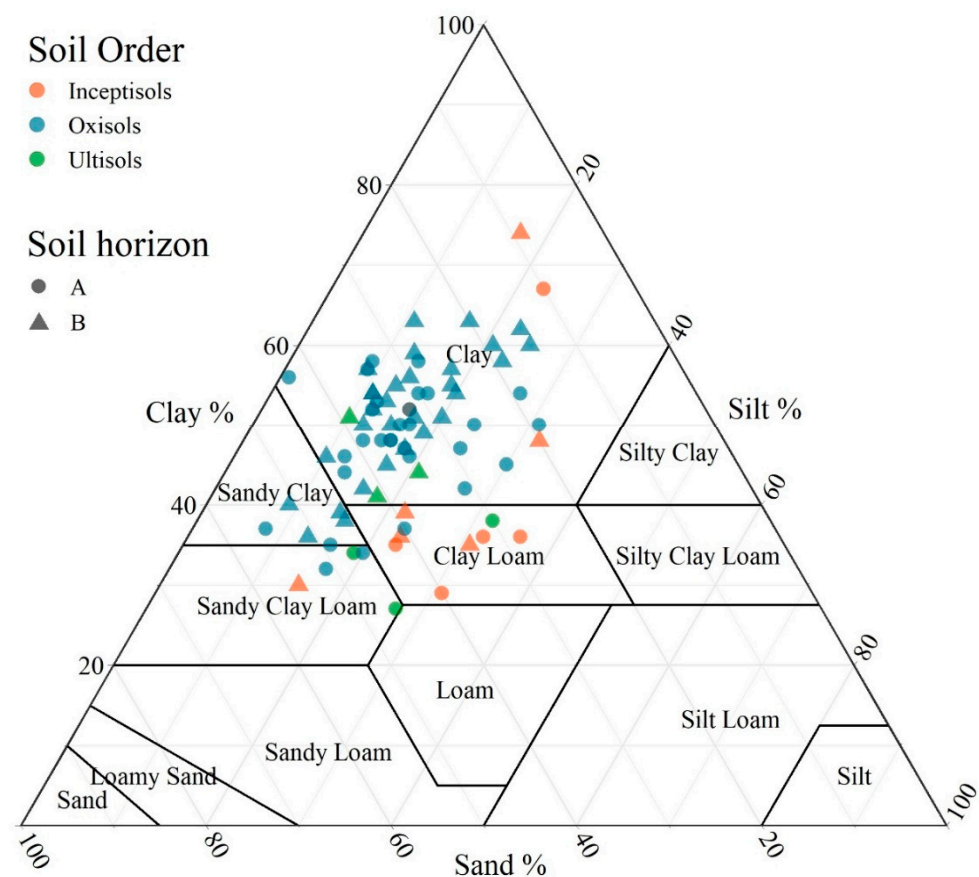


Figure 3. Soil textural classes, associated soil orders per US Soil Taxonomy [61], and horizons at a farmland scale in Brazil.

Soil characterization data obtained by pXRF are shown in Table 3. The main elements present in these soils were Al, followed by Si and Fe, in accordance with the results found by Lima et al. [66] and Teixeira et al. [67] in Brazilian soils. While Si tends to accumulate in these soils mainly as part of the crystalline structure of quartz and muscovite in the sand and silt fractions, and of kaolinite in the clay fraction, Fe and Al tend to concentrate in the clay fraction in the form of Fe and Al oxide minerals, beyond kaolinite in the case of Al [68]. Mobile elements that have low natural contents in most Brazilian soils [60] such as Ca, also presented large variability. Calcium content is increased with a liming application, which is

commonly performed in most Brazilian soils [2]. Accordingly, greater Ca contents were observed in A horizon samples. The other elements quantified by pXRF presented varied contents as a consequence of different soil horizons, soil classes, parent materials, and land uses of the study area.

Magnetic susceptibility values were greater in B horizons in association with the greater content of Fe oxide minerals in these horizons. Magnetite in the sand and silt fractions and maghemite in the clay fraction were commonly observed [69].

3.2. Prediction Model Performance for Available Micronutrients and Texture

The accuracy of prediction models is presented in Figure 4 (R^2) and Figure 5 (RMSE). For soil texture, the best prediction models were achieved with datasets including pXRF data alone or in association with other proximal or remote sensor data, i.e., MS + pXRF for sand content ($R^2 = 0.69$); TA + pXRF for silt content ($R^2 = 0.40$); and pXRF alone for clay content ($R^2 = 0.67$). The best results were achieved in B horizons for sand and clay, while for silt, optimal results were afforded by the A + B horizons dataset. The TA may have improved the performance of silt content prediction models since soils presenting more silt content tend to occur in steep relief conditions [57,58,70], which cannot be captured by pXRF elemental data ($R^2 = 0.22$ for A + B horizons dataset). Depending on soil mineralogy, MS data have been strongly correlated with sand and clay contents, especially when they present magnetic minerals [15,23,71]. Additionally, pXRF data alone have already been successfully used to predict soil texture in different parts of the world confirming the potential application of this proximal sensor for such prediction [23,56,72,73]. Silva et al. [56] predicted clay, silt, and sand contents from pXRF data in Brazil using ~1600 soil samples. The best predictions were delivered by support vector machine and RF, reaching R^2 values of 0.83 for clay (both algorithms), 0.70 and 0.75 for silt, and 0.87 and 0.84 for sand, respectively.

Similar to soil texture, optimal results were delivered when pXRF data were included in prediction models for available Cu (pXRF alone), Fe (MS + pXRF) using B horizon data, and Mn (TA + pXRF + MS) using A horizon data. For available B and Zn, superior results were achieved with TA data alone in the A + B horizons dataset. The importance of TA data for the prediction of available micronutrient content was previously reported [10], mostly by topography correlations with water dynamics and redoximorphic processes. In that study, the best models to predict available Cu, Fe, and Mn and Zn content included pXRF data and reached R^2 values of 0.74, 0.86, 0.71, respectively. Comparatively, studies developed in Sub-Saharan Africa were able to predict available B, Fe, and Mn content with moderate accuracy using GIS information [50]. For available B, Fe, and Mn content, the authors found R^2 values of 0.41, 0.68, and 0.53, respectively. Shahbazi et al. [74] predicted available B contents at different soil depths in Northwest Iran using GIS information, yet with a low R^2 value.

The different datasets grouped per soil horizons (A, B, or A + B) delivered variable results also depending on the prediction variables selected. For instance, using only pXRF data, A horizons provided the greatest R^2 value for Mn and the lowest R^2 value for available Fe. An opposite trend was found when using B horizon data. Additionally, the best predictions for available B and Zn as well as silt content were achieved by A + B horizons data. Thus, it was not possible to indicate if specific models per horizon or a general model combining both horizons' data would provide better results under universal conditions. Although other works attempting to predict soil attributes have suggested the creation of more specific models to increase some prediction results [13], the present study indicates prediction model performance regarding different datasets may depend upon the soil attribute being evaluated. In addition, soil attributes may behave differently due to site-specific variability [75].

Table 2. Descriptive statistics of available micronutrient contents and texture of soil horizons at a farmland scale in Brazil.

Attribute	Soil Horizon	n ^a	Min ^b	Max ^c	Mean	SD ^d	CV ^e %
B	A	39	0.03	0.22	0.11	0.05	45.45
	B	39	0.02	0.22	0.08	0.05	62.50
	A + B	78	0.02	0.22	0.10	0.05	50.00
Cu	A	39	0.18	4.08	0.84	0.73	86.90
	B	39	0.10	2.57	0.71	0.52	73.24
	A + B	78	0.10	4.08	0.78	0.64	82.05
Fe	A	39	17.99	230.24	63.89	52.89	82.78
	B	39	14.09	343.02	49.47	57.91	117.06
	A + B	78	14.09	343.02	56.68	55.57	98.04
Mn	A	39	8.35	180.55	32.95	33.02	100.21
	B	39	1.08	72.46	10.01	12.71	126.97
	A + B	78	1.08	180.55	21.48	27.40	127.56
Zn	A	39	0.49	86.63	7.87	13.47	171.16
	B	39	0.10	4.79	1.05	1.09	103.81
	A + B	78	0.10	86.63	4.46	10.09	226.23
(%)							
Clay	A	39	27	67	46	9	20
	B	39	30	74	50	9	19
	A + B	78	27	74	48	10	20
Silt	A	39	1	36	19	8	41
	B	39	9	32	17	6	33
	A + B	78	1	36	18	7	38
Sand	A	39	10	55	35	9	26
	B	39	9	55	33	10	32
	A + B	78	9	55	34	10	29

^a Number of samples, ^b minimum, ^c maximum, ^d standard deviation, ^e coefficient of variation.

Table 3. Descriptive statistics of portable X-ray fluorescence (pXRF) spectrometer (mg kg⁻¹) and magnetic susceptibility (MS) ($\times 10^{-6}$ m³ kg⁻¹) data per soil horizon at a farmland scale in Brazil.

Element	A Horizon					B Horizon				
	Min ^a	Max ^b	Mean	SD ^c	CV ^d	Min	Max	Mean	SD	CV
Al	44,781	105,232	72,441	16,494	23	49.65	98.17	70,835	11,898	17
As	6	38	13	5	41	8	24	14	4	26
Ca	<LOD ^e	3742	1082	896	83	<LOD	2018	117	390	334
Cr	56	150	81	18	22	52	150	85	24	28
Cu	16	59	28	8	29	17	44	27	7	25
Fe	24,863	68,014	43,567	9604	22	27,261	75,936	47,983	10,812	23
K	<LOD	15,245	4772	4765	100	<LOD	15,194	4189	4399	105
Mn	68	1.45	238	263	110	64	947	176	187	106
Ni	16	42	28	7	24	14	55	30	11	36
P	<LOD	1602	664	342	51	74	777	351	162	46
Pb	9	37	19	6	32	6	32	19	6	34
Rb	7	112	38	31	80	5	122	38	32	85
S	<LOD	635	242	120	49	<LOD	233	85	67	78
Si	41,149	14,4397	70,634	21,794	31	39,146	116,214	65,331	20,403	31
Sr	10	74	30	17	56	8	81	27	19	69
Ti	6052	10,970	8385	1.37	16	5144	10,829	8369	1578	19
V	36	98	68	14	20	41	94	69	15	22
Y	9	22	14	3	21	7	24	15	3	23
Zn	28	284	62	48	77	22	81	43	16	37
MS	2	57	13	11	83	2	75	15	14	95

^a Min—minimum value; ^b Max—maximum value; ^c SD—standard deviation; ^d CV—coefficient of variation; ^e LOD—limit of detection.

Notably, datasets including pXRF data (TA + pXRF, TA + MS + pXRF, MS + pXRF, and pXRF alone) provided the best predictions using B horizon data, while datasets including TA data without pXRF (TA alone and TA + MS) achieved the best predictions for A + B horizons data. Considering all the soil attributes studied, no well-defined pattern could be identified regarding the inclusion of either proximal or remotely sensed variables in the datasets regarding the achievement of the best prediction models. The best prediction models per soil attribute were reached using: TA dataset and A + B horizons data for available B and Zn content; pXRF data alone and B horizon data for available Cu and clay content; MS + pXRF data and B horizon data for available Fe and sand content; TA + pXRF + MS data and A horizon data for available Mn content; and TA + pXRF data and A + B horizons data for silt content.

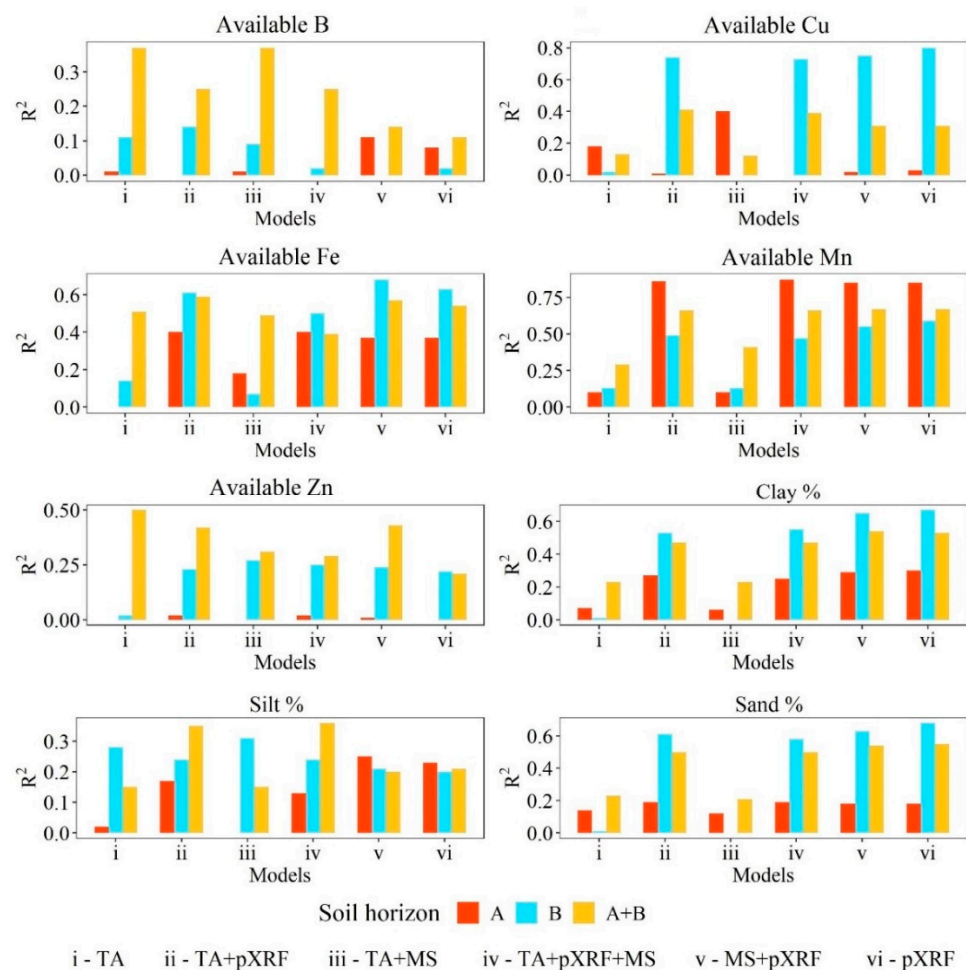


Figure 4. Coefficient of determination (R^2) for available B, Cu, Fe, Mn, and Zn, and clay, silt, and sand fraction prediction models via random forest algorithm for A, B, and A + B horizons at a farmland scale in Brazil. TA—terrain attributes, pXRF—portable X-ray fluorescence; MS—magnetic susceptibility.

Although TA data have been extensively used as predictor variables for soil attributes [47,50,76–79], they do not always substantially improve the model performance. Per Nolan et al. [80], TAs alone cannot account for many factors that affect soil fertility, especially when considering ameliorant application. Additionally, TAs are more important when dealing with areas more homogeneous in terms of soil classes and parent materials. However, terrain information has the advantage of being freely available and easily obtained. Their combination with other auxiliary data (e.g., proximal sensor data) can potentially improve model performance and precision soil management [15,81].

Given the aforementioned results, one can establish an ascending order of accuracy. Therefore, the groups are: (a) R^2 ranging from 0.37 to 0.50 for available B (0.37), Zn (0.50)

and silt (0.40) content; (b) R^2 ranging from 0.60 to 0.70 for available Fe (0.68), clay (0.67), and sand (0.69) content; and (c) R^2 ranging from 0.80 to 0.87 for Cu (0.80) and Mn (0.87) content. In digital soil mapping, accuracies of $R^2 > 70\%$ are considered good results (although very difficult to be achieved); accuracies of $R^2 < 50\%$ are more common [82,83]. Herein, at least one adequate predictive model was obtained for most soil attributes. Thus, the best models per soil attribute were used to generate spatial prediction maps.

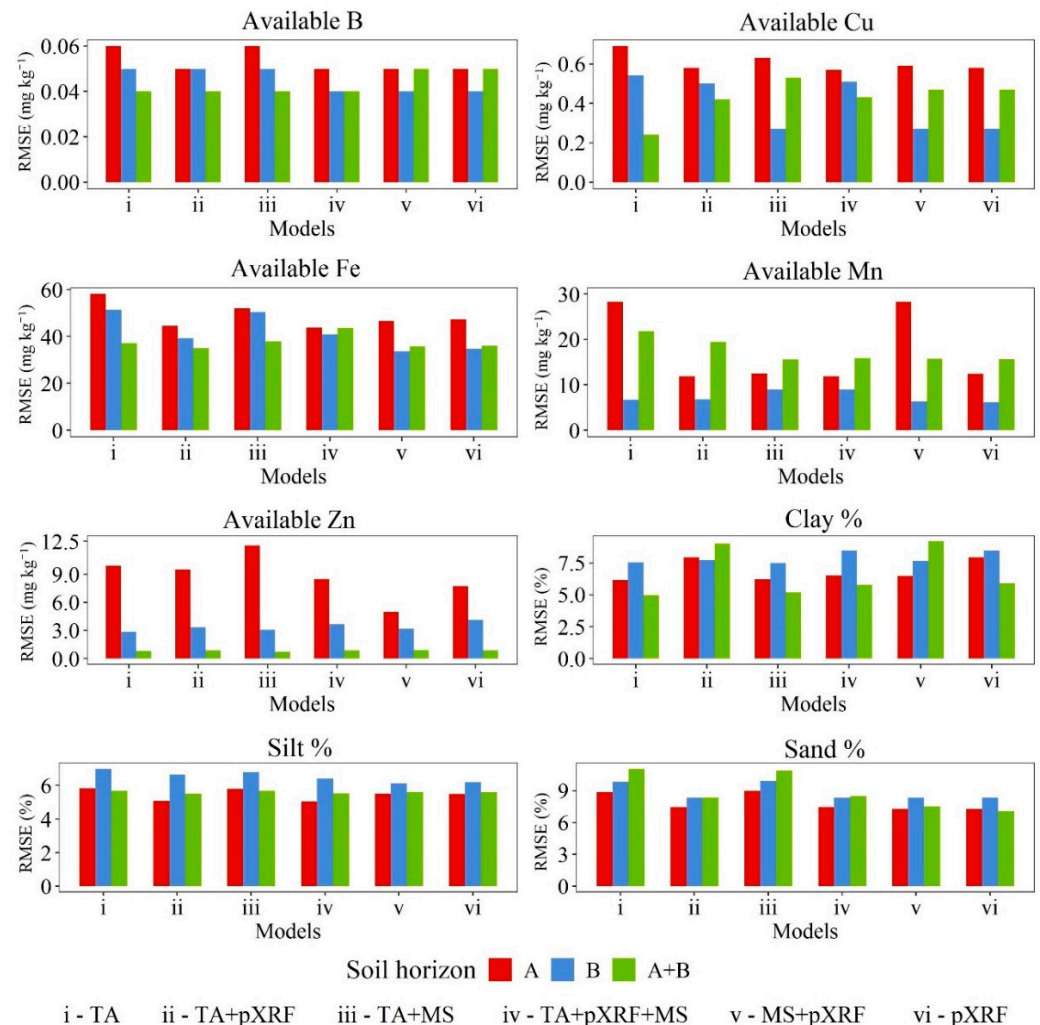


Figure 5. Root mean square error (RMSE) for available B, Cu, Fe, Mn, and Zn, and clay, silt, and sand fraction prediction models via random forest algorithm for A, B, and A + B horizons at a farmland scale in Brazil. TA—terrain attributes, pXRF—portable X-ray fluorescence; MS—magnetic susceptibility.

3.3. Variable Importance

The combination of the six datasets [i: TA; ii: TA + pXRF; iii: TA + MS; iv: TA + MS + pXRF; v: MS + pXRF; vi: pXRF] and the data for A, B, or A + B horizons resulted in a total of 144 models for the prediction of the soil micronutrient availability and particle size fractions. The best models to predict available B, Cu, Fe, Mn, Zn, and clay, silt, and sand contents had their variable importance calculated by the percentage of increment of Mean Square Error (%IncMSE) and were chosen with deference to highest R^2 and smallest RMSE. Figure 6 shows the five most essential variables per model.

For clay, silt, and sand, the most stable elements in the soil profile such as Al, Si, and Ti [21] presented their greatest importance in models using B horizon data. The best variables were provided by pXRF data, except for B and Zn as their best models used only TA data. This may occur due to the relationship between micronutrients and their exchangeable/available and elemental forms in soils [23]. For available Cu and Mn,

among the five most essential variables were Zn, Mn, and Cu. For Fe, the most important variables were Rb, K, MS, Zn, and Mn. The use of MS information may have improved Fe prediction reflecting magnetite (coarse fractions) and maghemite (clay fractions) minerals with magnetism. For B, the most essential variable was the closed depression (CD), the different horizons the samples were collected (Hor), valley depth (VD), relative slope position (RSP), and flow accumulation (Flow). For the available Zn, the most important variables were the different horizons the samples were collected (Hor), and land use, indicating the land uses of the study area, followed by catchment slope (CS), modified catchment area (MCA), and SAGA wetness index (SWI).

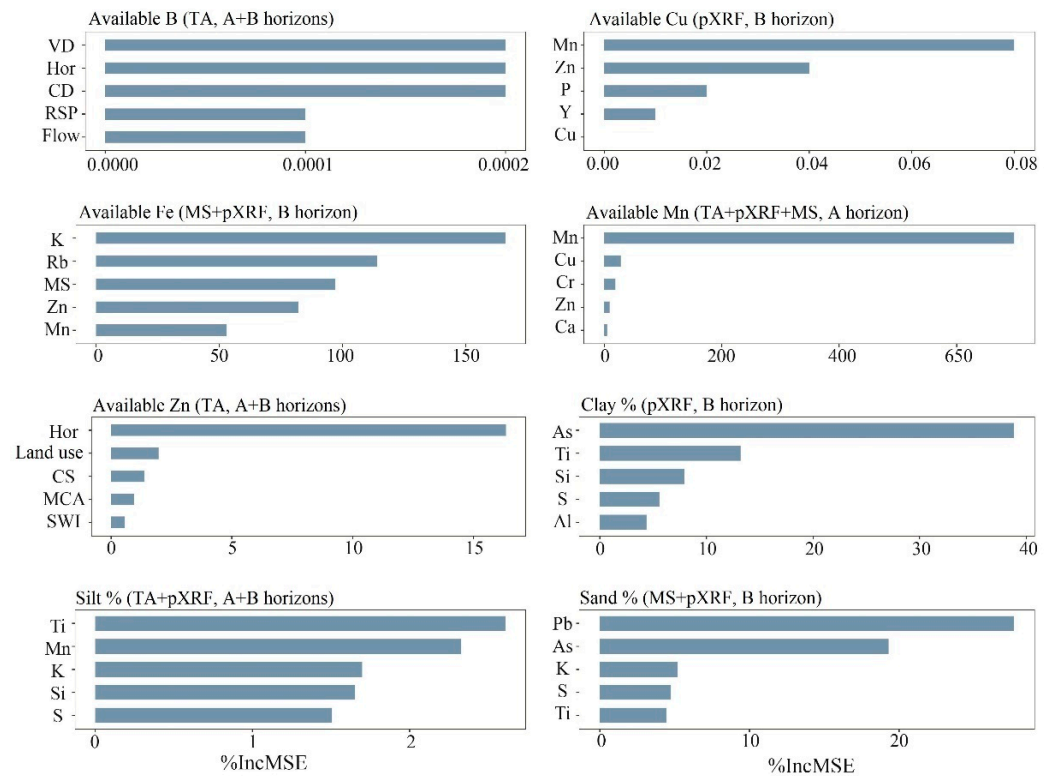


Figure 6. Plots of the five most essential variables for the best RF prediction models to predict soil available micronutrient and texture at a farmland scale in Brazil. pXRF, portable X-ray fluorescence; VD, valley depth; CD, closed depressions; CNBL, channel network base level; RSP, relative slope position; flow, flow accumulation; CS, catchment slope; MCA, modified catchment area; SWI, SAGA wetness index; MS, magnetic susceptibility; Hor, soil horizon; Land use, land uses of the area.

Among the most important variables for models built with pXRF in the current study, Mn and Zn were highly relevant for predictions of micronutrients. For texture prediction, the most important variables were As, K, Mn, S, Si, and Ti, likely related to the chemical composition of the soils studied. Mn oxide is an abundant clay mineral in tropical soils due to intense weathering–leaching processes [84]. Similarly, the high reactivity of Zn with soil minerals favors its adsorption in soils with greater clay contents (Figure 3) [73,85,86]. These facts may explain, at least partially, the importance of these elements for the models predicting micronutrient availability to plants.

3.4. Spatial Prediction of Soil Properties

The spatial prediction of soil properties based on optimal prediction models determined in the previous section is shown in Figure 7. The spatial predictions were made only for the attributes that attained adequate validation (available Cu, Fe, and Mn, as well as sand and clay content). The maps were generated for the soil horizon with greater accuracy (A horizon for Mn, and B horizon for Cu, Fe, clay, and sand content).

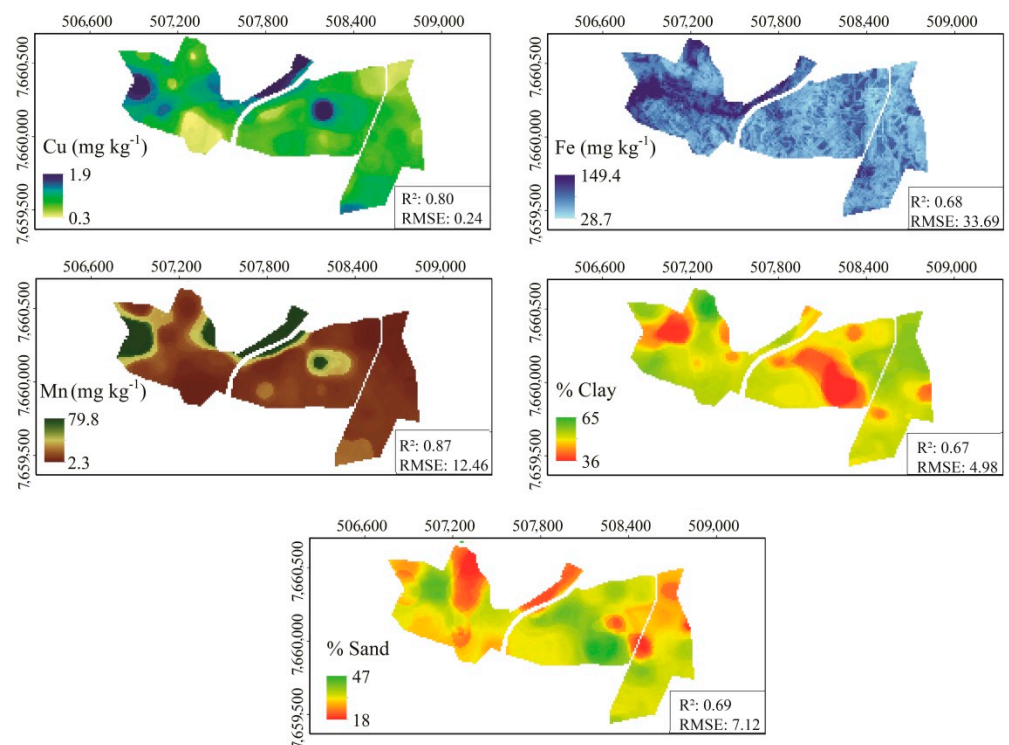


Figure 7. Maps of available B, Cu, Fe, Mn, and Zn, and clay, silt, and sand fraction content for A and B horizons obtained from optimal prediction models through random forest algorithm at a farmland scale in Brazil.

As expected, maps of sand and clay content present opposite trends. Since most Brazilian soils present low silt and higher clay or sand contents [4,56], sites containing greater clay simultaneously contain lower sand content. Most soils of the area are Oxisols, which are homogeneous in terms of soil texture throughout the soil profile. In the northwest part of the farm, Inceptisols feature greater sand content.

Micronutrient distribution could not be directly related to land use or soil class. This was likely caused by the different management practices applied in varied portions of the area, irrespective of soil class and land use distribution. For instance, areas containing the same soil class and land use may be subjected to different management practices, contributing to available micronutrient content variability on the farm. Despite that, maps delivered by this modeling approach enhanced the visualization of soil attribute variability with lower cost and informed the most appropriate management practice (e.g., application of soil ameliorants at variable rates) for each portion of the farm [13,87].

4. Conclusions

Soils were successfully characterized using proximal sensors. Satisfactory prediction results were obtained, allowing for accurate soil attribute mapping. Data from pXRF were present (alone or combined) in all the best prediction models, showing the importance of this sensor in prediction performance. The best sensor combinations for texture predictions were: MS + pXRF for sand content, TA + pXRF for silt content, and pXRF alone for clay content. Similarly, for micronutrients available to plants, the best sensor combinations were: pXRF alone for Cu, MS + pXRF for Fe, and TA + pXRF + MS for Mn. There was not a well-defined combination pattern for delivering the best prediction model for available micronutrients and texture regarding the combination of sensors and soil A and B horizons separately or merged into a single dataset. Satisfactory predictions were obtained for available Cu, Fe, and Mn (R² of 0.80, 0.68, and 0.87, respectively), as well as for clay and sand contents (R² of 0.67 and 0.69, respectively), with the use of an RF algorithm for at least one dataset. Maps showing the spatial variability of the best-predicted soil attributes can

enhance soil management decisions, requiring fewer samples for conventional laboratory analyses. For highly variable areas, combining proximal and remotely sensed data is recommended for digital mapping and modeling of soil properties in greater detail.

Author Contributions: Conceptualization, S.H.G.S., R.A., M.D.d.M., J.J.M. and D.C.W.; methodology, L.M.P.P., S.H.G.S., R.A., M.D.d.M. and J.J.M.; software, L.M.P.P. and R.A.; validation, L.M.P.P. and R.A.; formal analysis, A.F.d.S.T. and M.M.; investigation, L.M.P.P., A.F.d.S.T. and R.A.; writing—original draft preparation, L.M.P.P.; writing—review and editing, L.M.P.P., S.H.G.S., A.F.d.S.T., M.M., R.A., M.D.d.M., J.J.M., D.C.W. and N.C.; visualization, L.M.P.P., A.F.d.S.T. and R.A.; supervision, S.H.G.S., D.C.W. and N.C.; project administration, S.H.G.S., D.C.W. and N.C. All authors have read and agreed to the published version of the manuscript.

Funding: This research was funded by the National Council for Scientific and Technological Development (CNPq), Coordination for the Improvement of Higher Education Personnel (CAPES), and the Foundation for Research of the State of Minas Gerais (FAPEMIG).

Data Availability Statement: Data can be requested from the corresponding authors.

Conflicts of Interest: The authors declare no conflict of interest.

References

1. Fageria, N.K.; Stone, L.F. Micronutrient Deficiency Problems in South America. In *Micronutrient Deficiencies in Global Crop Production*; Springer: Dordrecht, The Netherlands, 2008; pp. 245–266.
2. Lopes, A.S.; Guilherme, L.R.G. A Career Perspective on Soil Management in the Cerrado Region of Brazil. In *Advances in Agronomy*; Elsevier: Amsterdam, The Netherlands, 2016; Volume 137, pp. 1–72, ISBN 9780128046920.
3. da Silva, R.d.C.F.; da Silva, F.B.V.; Biondi, C.M.; do Nascimento, C.W.A.; de Oliveira, E.C.A. Assessing the Content of Micronutrients in Soils and Sugarcane in Different Pedogeological Contexts of Northeastern Brazil. *Rev. Bras. Ciência Solo* **2019**, *43*, e0180228. [[CrossRef](#)]
4. Resende, M.; Curi, N.; Rezende, S.B.; Corrêa, G.F.; Ker, J.C. *Pedologia: Base Para Distinção de Ambientes*, 6th ed.; Editora UFLA: Lavras, Brazil, 2014.
5. Huuskonen, J.; Oksanen, T. Soil Sampling with Drones and Augmented Reality in Precision Agriculture. *Comput. Electron. Agric.* **2018**, *154*, 25–35. [[CrossRef](#)]
6. Adams, M.L.; Cook, S.; Bowden, J.W. Using Yield Maps and Intensive Soil Sampling to Improve Nitrogen Fertiliser Recommendations from a Deterministic Model in the Western Australian Wheatbelt. *Aust. J. Exp. Agric.* **2000**, *40*, 959–968. [[CrossRef](#)]
7. Takele, C.; Iticha, B. Use of Infrared Spectroscopy and Geospatial Techniques for Measurement and Spatial Prediction of Soil Properties. *Heliyon* **2020**, *6*, e05269. [[CrossRef](#)]
8. Mulla, D.J. Twenty Five Years of Remote Sensing in Precision Agriculture: Key Advances and Remaining Knowledge Gaps. *Biosyst. Eng.* **2013**, *114*, 358–371. [[CrossRef](#)]
9. Duda, B.M.; Weindorf, D.C.; Chakraborty, S.; Li, B.; Man, T.; Paulette, L.; Deb, S. Soil Characterization across Catenas via Advanced Proximal Sensors. *Geoderma* **2017**, *298*, 78–91. [[CrossRef](#)]
10. Pelegrino, M.H.P.; Weindorf, D.C.; Silva, S.H.G.; de Menezes, M.D.; Poggere, G.C.; Guilherme, L.R.G.; Curi, N. Synthesis of Proximal Sensing, Terrain Analysis, and Parent Material Information for Available Micronutrient Prediction in Tropical Soils. *Precis. Agric.* **2019**, *20*, 746–766. [[CrossRef](#)]
11. Ribeiro, B.T.; Silva, S.H.G.; Silva, E.A.; Guilherme, L.R.G. Portable X-Ray Fluorescence (PXRF) Applications in Tropical Soil Science. *Ciência Agrotecnologia* **2017**, *41*, 245–254. [[CrossRef](#)]
12. Weindorf, D.C.; Bakr, N.; Zhu, Y. Advances in Portable X-Ray Fluorescence (PXRF) for Environmental, Pedological, and Agronomic Applications. *Adv. Agron.* **2014**, *128*, 1–45. [[CrossRef](#)]
13. Benedet, L.; Acuña-Guzman, S.F.; Faria, W.M.; Silva, S.H.G.; Mancini, M.; Teixeira, A.F.D.S.; Pierangeli, L.M.P.; Acerbi Júnior, F.W.; Gomide, L.R.; Pádua Júnior, A.L.; et al. Rapid Soil Fertility Prediction Using X-Ray Fluorescence Data and Machine Learning Algorithms. *Catena* **2021**, *197*, 105003. [[CrossRef](#)]
14. Dijair, T.S.B.; Silva, F.M.; Teixeira, A.F.d.S.; Silva, S.H.G.; Guilherme, L.R.G.; Curi, N. Correcting Field Determination of Elemental Contents in Soils via Portable X-Ray Fluorescence Spectrometry. *Ciência Agrotecnologia* **2020**, *44*, e002420. [[CrossRef](#)]
15. Silva, S.H.G.; Poggere, G.C.; Menezes, M.D.; Carvalho, G.S.; Guilherme, L.R.G.; Curi, N. Proximal Sensing and Digital Terrain Models Applied to Digital Soil Mapping and Modeling of Brazilian Latosols (Oxisols). *Remote Sens.* **2016**, *8*, 614. [[CrossRef](#)]
16. Tavares, T.R.; Molin, J.P.; Nunes, L.C.; Alves, E.E.N.; Melquiades, F.L.; Carvalho, H.W.P.; Mouazen, A.M. Effect of X-ray Tube Configuration on Measurement of Key Soil Fertility Attributes with XRF. *Remote Sens.* **2020**, *12*, 963. [[CrossRef](#)]
17. Teixeira, A.F.d.S.; Silva, S.H.G.; Soares de Carvalho, T.; Silva, A.O.; Azarias Guimarães, A.; de Souza Moreira, F.M. Soil Physicochemical Properties and Terrain Information Predict Soil Enzymes Activity in Phytophysiologicals of the Quadrilátero Ferrífero Region in Brazil. *Catena* **2021**, *199*, 105083. [[CrossRef](#)]

18. Vasques, G.M.; Rodrigues, H.M.; Coelho, M.R.; Baca, J.F.M.; Dart, R.O.; Oliveira, R.P.; Teixeira, W.G.; Ceddia, M.B. Field Proximal Soil Sensor Fusion for Improving High-Resolution Soil Property Maps. *Soil Syst.* **2020**, *4*, 52. [[CrossRef](#)]
19. Curi, N.; Silva, S.H.G.; Poggere, G.C.; de Menezes, M.D. *Mapeamento de Solos e Magnetismo No Campus Da UFLA Como Traçadores Ambientais*, 1st ed.; Editora UFLA: Lavras, Brazil, 2017; Volume 1.
20. Cervi, E.C.; da Costa, A.C.S.; de Souza Junior, I.G. Magnetic Susceptibility and the Spatial Variability of Heavy Metals in Soils Developed on Basalt. *J. Appl. Geophys.* **2014**, *111*, 377–383. [[CrossRef](#)]
21. Mancini, M.; Weindorf, D.C.; Silva, S.H.G.; Chakraborty, S.; Teixeira, A.F.d.S.; Guilherme, L.R.G.; Curi, N. Parent Material Distribution Mapping from Tropical Soils Data via Machine Learning and Portable X-Ray Fluorescence (PXRF) Spectrometry in Brazil. *Geoderma* **2019**, *354*, 113885. [[CrossRef](#)]
22. Camargo, L.A.; Marques Júnior, J.; Pereira, G.T.; Bahia, A.S.R.D.S. Clay Mineralogy and Magnetic Susceptibility of Oxisols in Geomorphic Surfaces. *Sci. Agric.* **2014**, *71*, 244–256. [[CrossRef](#)]
23. Andrade, R.; Silva, S.H.G.; Faria, W.M.; Poggere, G.C.; Barbosa, J.Z.; Guilherme, L.R.G.; Curi, N. Proximal Sensing Applied to Soil Texture Prediction and Mapping in Brazil. *Geoderma Reg.* **2020**, *23*, e00321. [[CrossRef](#)]
24. Jenny, H. *Factors of Soil Formation: A System of Quantitative Pedology*; McGraw-Hill Book Co., Inc.: New York, NY, USA, 1941; ISBN 0486681289.
25. McBratney, A.B.; Mendonça, L.; Minasny, B. *On Digital Soil Mapping*; Elsevier: Amsterdam, The Netherlands, 2003; Volume 117, ISBN 0016-7061.
26. Moore, I.D.; Gessler, P.E.; Nielsen, G.A.; Peterson, G.A. Soil Attribute Prediction Using Terrain Analysis. *Soil Sci. Soc. Am. J.* **1993**, *57*, 443–452. [[CrossRef](#)]
27. Grunwald, S. Multi-Criteria Characterization of Recent Digital Soil Mapping and Modeling Approaches. *Geoderma* **2009**, *152*, 195–207. [[CrossRef](#)]
28. Adhikari, K.; Minasny, B.; Greve, M.B.; Greve, M.H. Constructing a Soil Class Map of Denmark Based on the FAO Legend Using Digital Techniques. *Geoderma* **2014**, *214–215*, 101–113. [[CrossRef](#)]
29. Fernandes, D.; Machado, T.; De Menezes, M.D.; Henrique, S.; Silva, G. Transferability, Accuracy, and Uncertainty Assessment of Different Knowledge-Based Approaches for Soil Types Mapping. *Catena* **2019**, *182*, 104134. [[CrossRef](#)]
30. Mbagal-Semgalawe, Z.; Folmer, H. Household Adoption Behaviour of Improved Soil Conservation: The Case of the North Pare and West Usambara Mountains of Tanzania. *Land Use Policy* **2000**, *17*, 321–336. [[CrossRef](#)]
31. Nawar, S.; Corstanje, R.; Halcro, G.; Mulla, D.; Mouazen, A.M. Delineation of Soil Management Zones for Variable-Rate Fertilization. *Adv. Agron.* **2017**, *143*, 175–245. [[CrossRef](#)]
32. Breiman, L. Random Forests. *Mach. Learn.* **2001**, *45*, 5–32. [[CrossRef](#)]
33. Chagas, C.d.S.; de Carvalho Junior, W.; Bhering, S.B.; Calderano Filho, B. Spatial Prediction of Soil Surface Texture in a Semiarid Region Using Random Forest and Multiple Linear Regressions. *Catena* **2016**, *139*, 232–240. [[CrossRef](#)]
34. Chakraborty, S.; Li, B.; Weindorf, D.C.; Deb, S.; Acree, A.; De, P.; Panda, P. Use of Portable X-Ray Fluorescence Spectrometry for Classifying Soils from Different Land Use Land Cover Systems in India. *Geoderma* **2019**, *338*, 5–13. [[CrossRef](#)]
35. Rawal, A.; Chakraborty, S.; Li, B.; Lewis, K.; Godoy, M.; Paulette, L.; Weindorf, D.C. Determination of Base Saturation Percentage in Agricultural Soils via Portable X-Ray Fluorescence Spectrometer. *Geoderma* **2019**, *338*, 375–382. [[CrossRef](#)]
36. Quéméneur, J.J.G.A.; Ribeiro, R.A.J.; Trow, F.V.P.; Paciullo, M. Geologia Da Folha Lavras. In *Projeto Sul de Minas; COMIG, UFMG, UFRJ/UERJ*: Belo Horizonte, Brazil, 2002; pp. 259–319.
37. Dantas, A.A.A.; De Carvalho, L.G.; Ferreira, E. Climatic Classification and Tendencies in Lavras Region, MG. *Ciência Agrotecnologia* **2007**, *31*, 1862–1866. [[CrossRef](#)]
38. Mehlich, A. *Determination of P, Ca, Mg, K, Na and NH₄*; North Carolina Soil Testing Division: Raleigh, NC, USA, 1953; p. 195.
39. Jackson, M.L. *Soil Chemical Analysis*; Prentice Hall, Inc.: Englewood Cliffs, NJ, USA, 1958; Volume 498.
40. Berger, K.C.; Truog, E. Boron Determination in Soils and Plants. *Ind. Eng. Chem. Anal. Ed.* **1939**, *11*, 540–545. [[CrossRef](#)]
41. Wolf, B. The Determination of Boron in Soil Extracts, Plant Materials, Composts, Manures, Water and Nutrient Solutions. *Commun. Soil Sci. Plant Anal.* **1971**, *2*, 363–374. [[CrossRef](#)]
42. Gee, G.W.; Bauder, J.W. Particle-Size Analysis. In *Methods of Soil Analysis: Part 1—Physical and Mineralogical Methods*; Soil Science Society of America, American Society of Agronomy: Madison, WI, USA, 1986; Volume 5, pp. 383–411. ISBN 978-0-89118-864-3.
43. Dearing, J. *Environmental Magnetic Susceptibility Using the Bartington MS2 System*, 2nd ed.; Chi Publishing: Kenilworth, UK, 1999; ISBN 0952340909.
44. Weindorf, D.C.; Chakraborty, S. Portable X-ray Fluorescence Spectrometry Analysis of Soils. *Soil Sci. Soc. Am. J.* **2020**, *84*, 1384–1392. [[CrossRef](#)]
45. Conrad, O.; Bechtel, B.; Bock, M.; Dietrich, H.; Fischer, E.; Gerlitz, L.; Wehberg, J.; Wichmann, V.; Böhner, J. System for Automated Geoscientific Analyses (SAGA) v. 2.1.4. *Geosci. Model Dev.* **2015**, *8*, 1991–2007. [[CrossRef](#)]
46. Adhikari, K.; Kheir, R.B.; Greve, M.B.; Bøcher, P.K.; Malone, B.P.; Minasny, B.; McBratney, A.B.; Greve, M.H. High-Resolution 3-D Mapping of Soil Texture in Denmark. *Soil Sci. Soc. Am. J.* **2013**, *77*, 860–876. [[CrossRef](#)]
47. Silva, S.H.G.; De Menezes, M.D.; Owens, P.R.; Curi, N. Retrieving Pedologist’s Mental Model from Existing Soil Map and Comparing Data Mining Tools for Refining a Larger Area Map under Similar Environmental Conditions in Southeastern Brazil. *Geoderma* **2016**, *267*, 65–77. [[CrossRef](#)]

48. Teixeira, A.F.S.; Silva, J.S.; Vilela, L.A.F.; Costa, P.F.; Costa, E.M.D.; Guimarães, A.A.; Santos, J.V.D.; Silva, S.H.G.; Carneiro, M.A.C.; Moreira, F.M.S. Microbiological Indicators of Soil Quality Under Native Forests Are Influenced by Topographic Factors. *An. Acad. Bras. Cienc.* **2019**, *91*, e20180696. [[CrossRef](#)]
49. Arrouays, D.; Grundy, M.G.; Hartemink, A.E.; Hempel, J.W.; Heuvelink, G.B.M.; Hong, S.Y.; Lagacherie, P.; Lelyk, G.; McBratney, A.B.; McKenzie, N.J.; et al. GlobalSoilMap: Toward a Fine-Resolution Global Grid of Soil Properties. In *Advances in Agronomy*; Elsevier: Amsterdam, The Netherlands, 2014; Volume 125, pp. 93–134, ISBN 9780128001370.
50. Hengl, T.; Leenaars, J.G.B.; Shepherd, K.D.; Walsh, M.G.; Heuvelink, G.B.M.; Mamo, T.; Tilahun, H.; Berkhout, E.; Cooper, M.; Fegraus, E.; et al. Soil Nutrient Maps of Sub-Saharan Africa: Assessment of Soil Nutrient Content at 250 m Spatial Resolution Using Machine Learning. *Nutr. Cycl. Agroecosyst.* **2017**, *109*, 77–102. [[CrossRef](#)]
51. Teixeira, A.F.d.S.; Weindorf, D.C.; Silva, S.H.G.; Guilherme, L.R.G.; Curi, N. Portable X-Ray Fluorescence (PXRF) Spectrometry Applied to the Prediction of Chemical Attributes in Inceptisols under Different Land Uses. *Ciência Agrotecnologia* **2018**, *42*, 501–512. [[CrossRef](#)]
52. R Core Team. *R: A Language and Environment for Statistical Computing*; R Foundation for Statistical Computing: Vienna, Austria, 2019.
53. Kuhn, M. Building Predictive Models in R Using the Caret Package. *J. Stat. Softw.* **2008**, *28*, 1–26. [[CrossRef](#)]
54. Liaw, A.; Wiener, M. Classification and Regression by RandomForest. *R News* **2002**, *2*, 18–22. [[CrossRef](#)]
55. Lee, S.; Wolberg, G.; Shin, S.Y. Scattered Data Interpolation with Multilevel B-Splines. *IEEE Trans. Vis. Comput. Graph.* **1997**, *3*, 228–244. [[CrossRef](#)]
56. Silva, S.H.G.; Weindorf, D.C.; Pinto, L.C.; Faria, W.M.; Acerbi Junior, F.W.; Gomide, L.R.; de Mello, J.M.; de Pádua Junior, A.L.; de Souza, I.A.; dos Santos Teixeira, A.F.; et al. Soil Texture Prediction in Tropical Soils: A Portable X-Ray Fluorescence Spectrometry Approach. *Geoderma* **2020**, *362*, 114136. [[CrossRef](#)]
57. Curi, N.; Silva, E.; Gomes, F.H.; Menezes, M.D.; Silva, S.H.G.; Teixeira, A.F.d.S. *Mapeamento de Solos, Aptidão Agrícola e Taxa de Adequação Do Uso Das Terras Do Município de Lavras (MG)*, 1st ed.; Editora UFLA: Lavras, Brazil, 2020; ISBN 9786586561050.
58. Curi, N.; Lima, J.M.; Andrade, H.; Gualberto, V. Geomorfologia, Física, Química e Mineralogia Dos Principais Solos Da Região de Lavras (MG). *Ciência Prática* **1990**, *14*, 297–307.
59. Marques Júnior, J.; Curi, N.; Lima, J.M. Evolução Diferenciada de Latossolo Vermelho-Amarelo e Latossolo Vermelho-Escuro Em Função Da Litologia Gnáissica Na Região de Lavras-MG. *Rev. Bras. Ciência Solo* **1992**, *26*, 235–240.
60. Resende, M.; Curi, N.; de Rezende, S.B.; Silva, S.H.G. *Da Rocha Ao Solo: Enfoque Ambiental*, 1st ed.; Editora UFLA: Lavras, Brazil, 2019.
61. Soil Survey Staff. *Keys to Soil Taxonomy*, 12th ed.; USDA: Washington, DC, USA, 2014.
62. Alvarez V, V.H.; Novais, R.F.; Barros, N.F.; Cantarutti, R.B.; Lopes, A.S. Interpretação Dos Resultados Das Análises de Solos. In *Recomendações Para o Uso de Corretivos e Fertilizantes em Minas Gerais: 5a Aproximação*; Comissão de Fertilidade do Solo do Estado de Minas Gerais – CFSEMG: Viçosa, Brazil, 1999; pp. 25–32.
63. Shukla, A.K.; Behera, S.K.; Lenka, N.K.; Tiwari, P.K.; Prakash, C.; Malik, R.S.; Sinha, N.K.; Singh, V.K.; Patra, A.K.; Chaudhary, S.K. Spatial Variability of Soil Micronutrients in the Intensively Cultivated Trans-Gangetic Plains of India. *Soil Tillage Res.* **2016**, *163*, 282–289. [[CrossRef](#)]
64. Zhu, H.; Zhao, Y.; Nan, F.; Duan, Y.; Bi, R. Relative Influence of Soil Chemistry and Topography on Soil Available Micronutrients by Structural Equation Modeling. *J. Soil Sci. Plant Nutr.* **2016**, *16*, 1038–1051. [[CrossRef](#)]
65. Zhu, H.; Hu, W.; Bi, R.; Peak, D.; Si, B. Scale- and Location-Specific Relationships between Soil Available Micronutrients and Environmental Factors in the Fen River Basin on the Chinese Loess Plateau. *Catena* **2016**, *147*, 764–772. [[CrossRef](#)]
66. de Lima, T.M.; Weindorf, D.C.; Curi, N.; Guilherme, L.R.G.; Lana, R.M.Q.; Ribeiro, B.T. Elemental Analysis of Cerrado Agricultural Soils via Portable X-Ray Fluorescence Spectrometry: Inferences for Soil Fertility Assessment. *Geoderma* **2019**, *353*, 264–272. [[CrossRef](#)]
67. Teixeira, A.F.d.S.; Henrique Procópio Pelegrino, M.; Missina Faria, W.; Henrique Godinho Silva, S.; Gabriela Marcolino Gonçalves, M.; Weimar Acerbi Júnior, F.; Rezende Gomide, L.; Linares Pádua Júnior, A.; de Souza, I.A.; Chakraborty, S.; et al. Tropical Soil PH and Sorption Complex Prediction via Portable X-Ray Fluorescence Spectrometry. *Geoderma* **2020**, *361*, 114132. [[CrossRef](#)]
68. Kämpf, N.; Marques, J.J.; Curi, N. Mineralogia de Solos Brasileiros. In *Pedologia Fundamentos*; SBCS: Viçosa, Brazil, 2012; p. 343.
69. Resende, M.; Curi, N.; Ker, J.C.; de Rezende, S.B. *Mineralogia de Solos Brasileiros: Interpretação e Aplicações*, 2nd ed.; Editora UFLA: Lavras, MG, Brazil, 2011; ISBN 9788587692252.
70. Curi, N.; Silva, S.H.G.; Poggere, G.C.; Menezes, M.D. *Mapeamento de Solos e Magnetismo No Campus Da UFLA*; UFLA: Lavras, Brazil, 2017.
71. Tatyanchenko, T.V.; Alekseeva, T.V.; Kalinin, P.I. Mineralogical and Chemical Compositions of the Paleosols of Different Ages Buried under Kurgans in the Southern Ergeni Region and Their Paleoclimatic Interpretation. *Eurasian Soil Sci.* **2013**, *46*, 341–354. [[CrossRef](#)]
72. Zhu, Y.; Weindorf, D.C.; Zhang, W. Characterizing Soils Using a Portable X-Ray Fluorescence Spectrometer: 1. Soil Texture. *Geoderma* **2011**, *167–168*, 167–177. [[CrossRef](#)]
73. Benedet, L.; Faria, W.M.; Silva, S.H.G.; Mancini, M.; Demattê, J.A.M.; Guilherme, L.R.G.; Curi, N. Soil Texture Prediction Using Portable X-Ray Fluorescence Spectrometry and Visible near-Infrared Diffuse Reflectance Spectroscopy. *Geoderma* **2020**, *376*, 114553. [[CrossRef](#)]

74. Shahbazi, F.; Hughes, P.; McBratney, A.B.; Minasny, B.; Malone, B.P. Evaluating the Spatial and Vertical Distribution of Agriculturally Important Nutrients—Nitrogen, Phosphorous and Boron—in North West Iran. *Catena* **2019**, *173*, 71–82. [[CrossRef](#)]
75. Faria, Á.J.G.D.; Silva, S.H.G.; Melo, L.C.A.; Andrade, R.; Mancini, M.; Mesquita, L.F.; Teixeira, A.F.D.S.; Guilherme, L.R.G.; Curi, N. Soils of the Brazilian Coastal Plains Biome: Prediction of Chemical Attributes via Portable X-Ray Fluorescence (PXRF) Spectrometry and Robust Prediction Models. *Soil Res.* **2020**, *58*, 683–695. [[CrossRef](#)]
76. McKay, J.; Grunwald, S.; Shi, X.; Long, R.F. Evaluation of the Transferability of a Knowledge-Based Soil-Landscape Model. In *Digital Soil Mapping: Bridging Research, Environmental Application, and Operation*; Boettinger, J.L., Howell, D.W., Moore, A.C., Hartemink, A.E., Kienast-Brown, S., Eds.; Springer: London, UK, 2010; pp. 165–178, ISBN 9789048188635.
77. Arrouays, D.; Lagacherie, P.; Hartemink, A.E. Digital Soil Mapping across the Globe. *Geoderma Reg.* **2017**, *9*, 1–4. [[CrossRef](#)]
78. Pelegrino, M.H.P.; Silva, S.H.G.; de Menezes, M.D.; da Silva, E.; Owens, P.R.; Curi, N. Mapping Soils in Two Watersheds Using Legacy Data and Extrapolation for Similar Surrounding Areas. *Ciência Agrotecnologia* **2016**, *40*, 534–546. [[CrossRef](#)]
79. Machado, D.F.T.; Silva, S.H.G.; Curi, N.; Menezes, M.D. de Soil Type Spatial Prediction from Random Forest: Different Training Datasets, Transferability, Accuracy and Uncertainty Assessment. *Sci. Agric.* **2019**, *76*, 243–254. [[CrossRef](#)]
80. Nolan, T.; Connolly, J.; Sall, C.; Cesar, J. Mixed Livestock Grazing in Diverse Temperate and Semi-Arid Environments. *Afr. J. Range Forage Sci.* **2000**, *17*, 10–21. [[CrossRef](#)]
81. Nawar, S.; Delbecq, N.; Declercq, Y.; De Smedt, P.; Finke, P.; Verdoodt, A.; Van Meirvenne, M.; Mouazen, A.M. Can Spectral Analyses Improve Measurement of Key Soil Fertility Parameters with X-Ray Fluorescence Spectrometry? *Geoderma* **2019**, *350*, 29–39. [[CrossRef](#)]
82. Stumpf, F.; Schmidt, K.; Goebes, P.; Behrens, T.; Schönbrodt-Stitt, S.; Wadoux, A.; Xiang, W.; Scholten, T. Uncertainty-Guided Sampling to Improve Digital Soil Maps. *Catena* **2017**, *153*, 30–38. [[CrossRef](#)]
83. Malone, B.P.; McBratney, A.B.; Minasny, B.; Laslett, G.M. Mapping Continuous Depth Functions of Soil Carbon Storage and Available Water Capacity. *Geoderma* **2009**, *154*, 138–152. [[CrossRef](#)]
84. Terra, F.S.; Demattê, J.A.M.; Viscarra Rossel, R.A. Proximal Spectral Sensing in Pedological Assessments: Vis-NIR Spectra for Soil Classification Based on Weathering and Pedogenesis. *Geoderma* **2018**, *318*, 123–136. [[CrossRef](#)]
85. Palleiro, L.; Patinha, C.; Rodríguez-Blanco, M.L.; Taboada-Castro, M.M.; Taboada-Castro, M.T. Metal Fractionation in Topsoils and Bed Sediments in the Mero River Rural Basin: Bioavailability and Relationship with Soil and Sediment Properties. *Catena* **2016**, *144*, 34–44. [[CrossRef](#)]
86. Silva, S.H.G.; Silva, E.A.; Poggere, G.C.; Guilherme, L.R.G.; Curi, N. Tropical Soils Characterization at Low Cost and Time Using Portable X-Ray Fluorescence Spectrometer (PXRF): Effects of Different Sample Preparation Methods. *Ciência Agrotecnologia* **2018**, *42*, 80–92. [[CrossRef](#)]
87. Vasu, D.; Singh, S.K.; Sahu, N.; Tiwary, P.; Chandran, P.; Duraisami, V.P.; Ramamurthy, V.; Lalitha, M.; Kalaiselvi, B. Assessment of Spatial Variability of Soil Properties Using Geospatial Techniques for Farm Level Nutrient Management. *Soil Tillage Res.* **2017**, *169*, 25–34. [[CrossRef](#)]